ELSEVIER

Polymer 43 (2002) 4967–4972

polymer

www.elsevier.com/locate/polymer

Polymorphism in polyamide 66/clay nanocomposites

Xiaohui Liu*, Qiuju Wu, Lars A. Berglund

Division of Polymer Engineering, Luleå University of Technology, Luleå 97187, Sweden

Received 15 August 2001; received in revised form 20 May 2002; accepted 22 May 2002

Abstract

Polyamide 66/clay nanocomposites (PA66CN) were prepared via melt compounding method by using a new kind of organophilic clay, which was obtained through co-intercalation of epoxy resin and quaternary ammonium into Na-montmorillonite. The silicate layers were dispersed homogeneously and nearly exfoliated in polyamide 66 (PA66) matrix. The introduction of silicate layers induced the appearance of the γ phase in PA66CN at room temperature, more clay loadings would amplify this phenomenon; the addition of clay also changed the structure of the α crystalline phase. The presence of silicate layers increased the crystallization rate and had a strong hetero phase nucleation effect on PA66 matrix. The lower Brill transition temperature of PA66CN can be attributed to the strong interaction between polyamide chains and surfaces of silicate layers.

Keywords: Polyamide 66/clay nanocomposite; Organophilic clay; Crystal structure

1. Introduction

In recent years, organic–inorganic nanometer composites have attracted great interest from researchers since they frequently exhibit unexpected hybrid properties synergistically derived from two components. One of the most promising composites systems would be hybrids based on organic polymers and inorganic clay minerals consisting of layered structure, which belong to the general family of 2:1 layered silicates [1]. Compared to their micro- and macro-counterparts and the pristine polymer matrix, polymer/clay nanocomposites (PCN) exhibit improved tensile strength and moduli [2–5], decreased thermal expansion coefficient [2], decreased gas permeability [2–5], increased swelling resistance [6], enhanced ion conductivity [7–9], flammability [10,11] and so on. Presumably the enhanced properties of PCN are due to the formed nanoscale structure, the large aspect ratio and large surface area of the layered silicates and the strong interaction between polymer molecular chains and layered silicate.

The unprecedented mechanical properties of PCN were first demonstrated by a group at the Toyota research center in Japan using Polyamide 6/clay nanocomposites [12–14]. Since then, many PCN systems have been investigated and prepared including those with the polymers, poly(ε-caprolactone) [15], poly(methyl methacrylate) [16], polyaniline [17–19], polypyrrole [20], polyimide [5,21,22], polystyrene [23,24], polyamide 6 [25,26], polyamide 12 [27], polypropylene [28], poly(ethylene oxide) [7,9,29–31], poly(*p*-phenylenevinylene) [32], epoxy [2,33,34], polyurethane [35,36], etc.

In principal, two different routes are possible for PCN. One route is the intercalation of monomers into layered silicate hosts. In most cases, the synthesis involves either intercalation of a suitable monomer and then exfoliating the layers by following polymerization. This approach is limited since neither a suitable monomer nor a compatible solvent system is always available. Polymer melt intercalation is a promising route to fabricate PCN by using a conventional extrusion process.

Polyamide 66 (PA66) is a kind of important engineering plastics. Despite polyamide 6 and polyamide 12/clay nanocomposites have been investigated by many researchers, there is no paper concerned about polyamide 66/clay nanocomposites (PA66CN) up to now. One target of this article is to report the melt intercalation of PA66CN by using a new kind of organophilic clay.

The polymorphic structures of polyamides result from the differential spatial arrangement in the hydrogen bonding between the oxygen in the carbonyl group of one polyamide molecular chain and the hydrogen attached to the nitrogen in the neighboring polyamide molecular chain [37]. The crystal structures observed in polyamide mainly fall into

* Corresponding author. Tel.: +46-920-491770; fax: +46-920-491084.
E-mail address: xiaohui.liu@mb.luth.se (X. Liu), xiaohuiliu9@yahoo.com (X. Liu).

0032-3861/01/$ - see front matter
PII: S0032-3861(02)00331-2

two categories: α crystalline phase and γ crystalline phase. The α phase consisted of planar sheets of hydrogen bonding chains with sheets stacked upon one another and displaced along the chain direction by a fixed amount. The γ phase has pleated sheets of methylene units with hydrogen bonding between sheets rather than within sheets. The principal structural difference between α and γ phase is that the amide-to-methylene dihedrals are near *trans* (164–168°) in α and nearly perpendicular to the peptide plane (~126°) in γ phase [38–41]. The α phase of PA66 is more stable than γ phase at room temperature.

Many semicrystalline polymers undergo phase transitions prior to melting. The crystal-to-crystal phase transition in PA66 was observed first in polyamide and known as Brill transition, which has been studied extensively [42–48]. Upon heating PA66, the room temperature triclinic structure, α phase, transforms into another triclinic structure, γ phase. The Brill transition in PA66 is clearly displayed in X-ray diffraction (XRD) study, as two prime strong diffractions at ~20° (200) and ~24° (002 + 202) merge into a single diffraction at the transition temperature [42].

Another target of this article is to clarify the possibility of the α and γ phases with the presence of silicate layers, to investigate the influence of silicate layers on the crystallization behaviors of PA66CN. Besides, we will also study the structural changes of PA66CN as a result of thermal annealing.

2. Experiment

2.1. Materials

Polyamide 66, Ultramid A3 used in this study was manufactured by BASF. The cation exchange capacity of Na-montmorillonite (Na-MMT) used in this study was 80 meq/100 g. The particle size was less then 20 μm. Epoxy resin ARALDITE GY 240, a diglycidyl ether of bisphenol A with a molecular weight of 360, was kindly supplied by Ciba-Geigy.

A novel kind of co-intercalation organophilic clay used in this study was prepared as follows in two steps: (1) 100 g (Na-MMT) was dispersed into 5000 ml of hot water using homogenizer. Hexadecyl trimethyl ammonium bromide (30 g) was dissolved into hot water and poured into the Na-MMT–water solution under vigorous stirring for 30 min to yield white precipitates. The precipitates were collected and washed by hot water three times, and then were ground into the size of 20 μm after thoroughly dried in a vacuum oven. The obtained precipitate was a kind of organophilic clay widely used in PCN field which was designated as PrE-MMT here; (2) 130 g PrE-MMT obtained in step 1 and 20 g epoxy resin GY 240 were mixed in a Haake Recorder 40 mixer for 1 h. Then the co-intercalation organophilic clay designated as E-MMT can be obtained.

A twin-screw extruder was used for the preparation of the nanocomposites. PA66 granules were dried in vacuum oven at 120 °C for 24 h prior to blending with organophilic clay. The temperature of the extruder was maintained at 270, 290, 290 and 280 °C from hopper to die, respectively. The screw speed was maintained at 180 rpm. After dried at 80 °C for 6 h, the obtained nanocomposites was injection molded to get test specimens.

2.2. Characterization

In order to eliminate the influence of specimen thickness, ca. 100 μm films of specimen were prepared for XRD as follows: The granules of PA66 or PA66CN were put between two glass slides, then heated in oil-bath up to 280 °C. After the granules entirely melted and stay at this temperature for 10 min to eliminate the heat history, a load was applied on the surfaces of slides to press the melted materials into thin films. The thin films were prepared under two kinds of cooling conditions: (1) cooled in oil-bath from 280 to 20 °C naturally; (2) quickly removed from 280 °C oil-bath and quenched in liquid nitrogen.

In order to investigate the Brill transition of PA66 and PA66CN, the films were annealed in oil-bath at different temperatures for 2 h, and then the films were removed and quenched in liquid nitrogen again to be tested by XRD.

In addition to the crystal structure, the nanometer characteristic of the product obtained was also verified by XRD. XRD patterns of the films were recorded by a Siemens D5000 X-ray diffractometer at room temperature. The Cu Kα radiation source was operated at 40 kV and 20 mA. Patterns were recorded by monitoring those diffractions that appeared from 1.5 to 30°. The scan speed was 2° min^{-1}.

DSC analyses were carried out using a Perkin–Elmer DSC-7 differential scanning calorimeter thermal analyzer. About 10 mg of the polymer sample was weighted very accurately in the aluminium DSC pan and placed in the DSC cell. It was heated from 30 to 300 °C at a rate of 10 °C/min under nitrogen atmosphere. The sample was kept for 10 min at this temperature to eliminate the heat history before cooling at a specified cooling rate. Constant cooling rate 2.5, 5, 10, 20, and 40 °C/min were applied. The thermograms were recorded and analyzed to estimate the crystallinities under non-isothermal conditions.

3. Results and discussion

3.1. Characterization of nanostructure

Fig. 1 shows the XRD patterns of Na-MMT, PrE-MMT, and E-MMT, respectively. Na-MMT presents a characteristic diffraction peak corresponding to (001) plane at 1.24 nm. PrE-MMT shows a 1.96 nm basal space in XRD pattern. The basal space of E-MMT is 3.77 nm. Compared

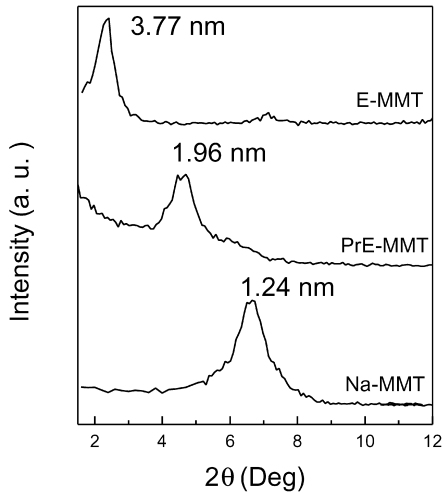

Fig. 1. XRD patterns of Na-MMT, PrE-MMT and E-MMT.

the 3.77 nm d_{001} value of E-MMT with the 1.24 nm d_{001} value of Na-MMT, the obviously increased layer distance demonstrates the advantage of the co-intercalation organophilic clay E-MMT.

The alkylammonium ion exchange enables conversion of the hydrophilic interior clay surface to hydrophobic and increases the layer distance as well. This is the condition of PrE-MMT. In this organophilic environment, epoxy resin is then diffusing into the clay galleries to increase the layer distance further. For this method applied with E-MMT we use the term co-intercalation. In addition to increasing layer distance, the co-intercalation clay also brings the active functional group into PA66 system; a good dispersion effect of E-MMT can be expected.

XRD patterns are used to evaluate the dispersion effect of clay in polymer matrix. The PA66 nanocomposite containing 1 wt% E-MMT is abbreviated as PA66CN1; similarly, the nanocomposites containing 3 and 5 wt% E-MMT are abbreviated as PA66CN3 and PA66CN5, respectively. As shown in Fig. 2, no obvious diffraction peak could be

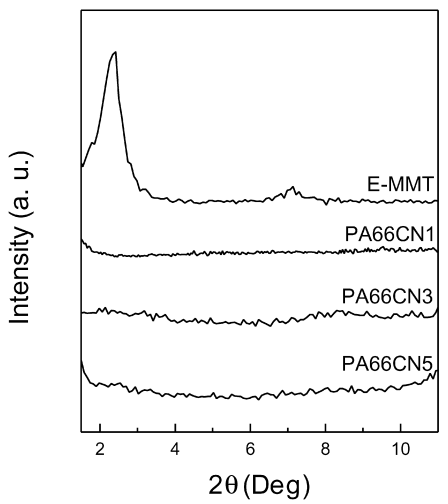

Fig. 2. XRD patterns of PA66CN with different E-MMT contents.

observed in PA66CN1, PA66CN3 and PA66CN5. The nearly disappeared peak of (001) plane in XRD pattern indicates that E-MMT has been dispersed homogeneously in PA66 matrix nearly exfoliated.

Giannelis [6] suggested that the confinement of the polymer inside the interlayers results in a decrease in the overall entropy of the polymer chains, at the same time, the entropic penalty of polymer confinement may be compensated by the increased conformational freedom of the tethered surfactant chains in a less confined environment as the layers separate. But their mean-field model also indicates that the entropy associated with the aliphatic chains only increases until the tethered chains are fully extended. Further layer separation depends on the establishment of very favorable interactions to overcome the continually increasing penalty of polymer confinement. Such intercalations must have caused the nearly exfoliated structure of PA66/E-MMT nanocomposites. First, the alkylammonium makes the silicate layers organophilic; then the presence of epoxy end group between the layers must attract PA66 molecules and cause strongly increased layer separation.

3.2. Crystal structures of PA66CN

Fig. 3(a) shows the XRD patterns of PA66 and PA66CN samples, which were slowly cooled to room temperature in oil-bath naturally after being melted into thin films at 280 °C. PA66 has various crystalline phases and usually presents the more stable α phase rather than the γ phase in XRD pattern. The two strong diffraction peaks at $2\theta = 20.4$ and 24.1° are the distinctive feature of the α phase of PA66, which are designated as α1 and α2, respectively. When adding 1 wt% E-MMT, the XRD pattern still shows only the presence of the α phase, however, the intensities of the α1 and α2 peaks have changed greatly. The α1 peak is dominant in PA66, while the α2 peak is much higher in PA66CN1. More clay loading induces the variation in crystal structures, some new diffraction peaks appear in PA66CN3, and this trend is amplified in PA66CN5. One can observe the high temperature structure γ phase which is unstable and seldom appears in PA66 at room temperature. The characteristic of the γ phase is a strong diffraction peak at $2\theta = 21.8°$, the diffraction peak at $2\theta = 13.6°$ is also contributed by the γ phase; they are designated as γ1 and γ2, respectively. In addition to the observation of the γ phase, in sharp contrast to PA66, the α1 diffraction peak diminishes greatly in PA66CN3 and PA66CN5.

Fig. 3(b) shows the XRD patterns of PA66 and PA66CN samples, which were immediately quenched in liquid nitrogen after being melted into thin films at 280 °C. Though the intensities are slightly lower than those of the slowly cooled PA66 sample, α1 and α2 are still the only diffraction peaks observed in the quenched PA66 sample. Unlike the slowly cooled sample in oil-bath, only 1 wt% clay loading induces the appearance of the γ phase when

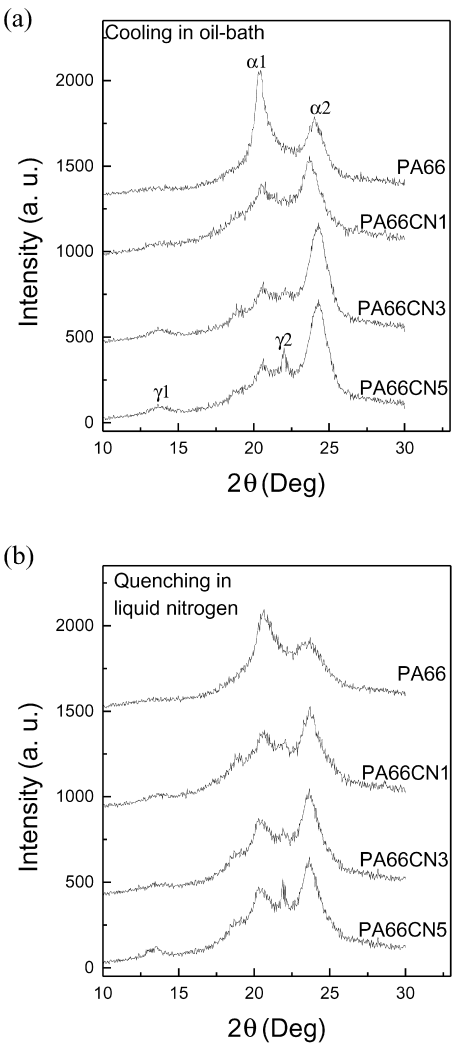

Fig. 3. XRD patterns of PA66 and PA66CN under different cooling conditions: (a) cooling in oil-bath; (b) quenching in liquid nitrogen.

PA66CN1 quenched in liquid nitrogen. The fractions of the γ phase increase in PA66CN when increasing clay loadings. Similar to the situation of the slowly cooled samples, the α2 diffraction peak becomes dominant in the quenched PA66CN samples. One can draw the following conclusions from above results: the introduction of silicate layers induces the appearance of the γ phase in PA66CN which is unstable and seldom appears in PA66 at room temperature, more clay loadings would amplify this phenomenon; the addition of clay also changes the structure of the α crystalline phase.

The α1 peak in XRD pattern of PA66 arises from the distance between hydrogen-bonded chains which is the diffraction of hydrogen bonded sheets, and the α2 peak arises from the separation of the hydrogen bond sheets [46]. The sharp decrease in intensity of the α1 peak in PA66CN indicates that the addition of clay disturbs the perfect arrangement of hydrogen bonded sheets of the α phase. This result also verifies the explanation to the appearance of the γ phase in PA66CN.

The similar phenomenon has been observed in polyamide 6 (PA6)/clay nanocomposites by many researchers [26,49–52], the addition of clay favors the formation of γ crystalline phase even using different preparation methods and various modified clays. Therefore, it is reasonable to ascribe this phenomenon to the interaction between clay layers and polymer chains. Vaia et al. [53] suggested an assumption to explain why the addition of clay causes the change in the crystalline phase of PA6 from predominantly α to largely γ phase. We think it is also reasonable to the case of PA66CN. They suggested that the proximity of the surface of layers results in conformation changes of chains, limiting the formation of hydrogen bonded sheets of the α phase, which can be verified by our above result that the α1 diffraction peak diminishes greatly in PA66CN, coordinating with the amide groups and forcing them out of the plane formed by the chains thus leading to the appearance of the γ crystalline phase. However, the α phase of PA66 is much more thermodynamically stable than that of PA6 at room temperature [41], that is the reason why the introduction of silicate layers results in just the appearance of γ phase in PA66 but the domination in PA6. The increase in the surfaces of layers, i.e. the increase in clay loadings, would increase the effective influence areas, thus more γ phases are induced in PA66CN.

3.3. Thermal behaviors of PA66CN

In order to obtain more information about the influence of silicate layers on melting and crystallization behaviors of PA66CN, non-isothermal thermal analyses are applied to these specimens. Fig. 4 shows the DSC heating scans of PA66, PA66CN1, PA66CN3, and PA66CN5, respectively, at a heating rate of 10 °C/min. PA66 has a melting temperature (T_m) at 260.9 °C. However, T_m of PA66CN occurs at slightly lower temperatures than that of PA66. This phenomenon may be related with the reduction in crystallite size in the presence of filler [54,55]. Non-isothermal crystallization experiments were operated by using the DSC cooling scans of PA66 and PA66CN at the

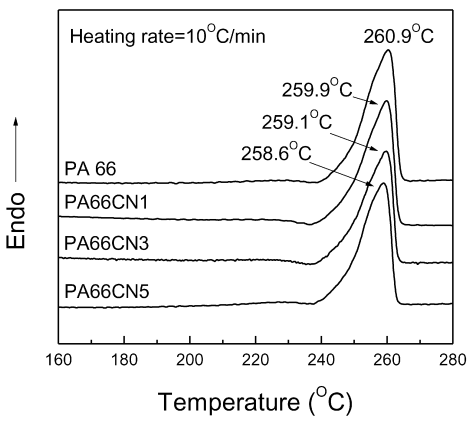

Fig. 4. DSC heating scans of PA66 and PA66CN (heating rate: 10 °C/min).

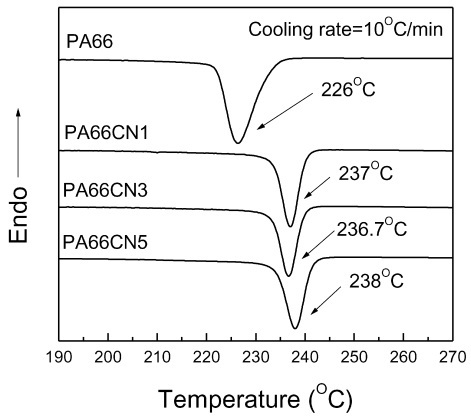

Fig. 5. DSC cooling scan of PA66 and PA66CN (cooling rate: 10 °C/min).

cooling rates of 2.5–40 °C/min. All the cooling scans have only one exothermic peak as the example shown in Fig. 5, which presents the DSC thermograms of PA66 and PA66CN cooled at 10 °C/min, but the peak forms and the peak temperatures of PA66CN differ from those of PA66. The peak and onset temperatures are listed in Table 1. It is obviously that the presence of silicate layers in the polymer matrix increases the crystallization temperatures and narrows the width of the crystalline peaks. These results indicate that the clay increases the crystallization rate and has a strong hetero phase nucleation effect on PA66 matrix. While in this case, more clay loadings do not accelerate the crystallization rate further; just 1 wt% clay content can prompt the crystallization behavior of PA66CN greatly.

3.4. Brill transition of PA66CN

A series of XRD scans of PA66 annealed at various temperatures are shown in Fig. 6(a). The XRD scans reflect the substantial changes in the structure as the sample is heated up. There are two crystalline diffractions at $2\theta = 20.4°$ ($\alpha 1$) and 24.1° ($\alpha 2$) at room temperature (20 °C). With increasing annealing temperature, the intensities of these two room-temperature peaks decrease. A new diffraction peak at $2\theta = 21.8°$ appears at ca. 170 °C, which is the only crystalline peak appeared at and above this temperature. This phenomenon is the well-known Brill transition of PA66, in which system two prime strong diffraction peaks merge into a single diffraction peak at a given temperature.

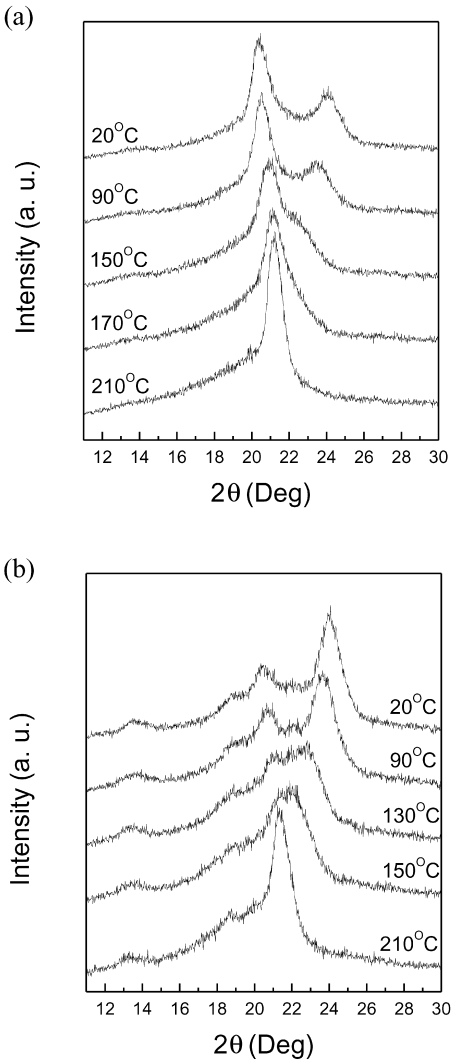

Fig. 6. XRD patterns of (a) PA66 and (b) PA66CN annealed at various temperatures.

The Brill transition can be attributed to the anisotropic thermal expansion. In this case, one can conclude that the Brill transition of PA66 is about 170 °C.

XRD scans of PA66CN3 (cooling with oil-bath) annealed at various temperatures are plotted in Fig. 6(b) as an example to present the Brill transition of PA66CN. At room temperature, in addition to the two crystalline diffraction peaks of the α phase, the γ phase also shows

Table 1
Peak and onset temperature of non-isothermal cooling scans of PA66 and PA66CN

Cooling (°C/min)	PA66		PA66CN1		PA66CN3		PA66CN5	
	T_p (°C)	T_o (°C)	T_p (°C)	T_o (°C)	T_p (°C)	T_o (°C)	T_p (°C)	T_o (°C)
2.5	234.5	241.3	243.0	247.1	243.2	248.3	244.8	248.9
5	230.2	238.7	241.3	246.8	242.1	245.2	241.9	246.8
10	226.0	235.8	237.0	244.3	236.7	243.8	238.0	243.4
20	220.1	233.8	233.6	242.2	232.3	241.0	234.3	242.2
40	213.4	229.3	226.3	237.5	224.1	235.3	226.4	237.4

its characteristic peak at $2\theta = 21.8°$. As in the case of PA66 under annealing, PA66CN3 also exhibits a crystalline transition from the α phase to the γ phase when it is heated up. However, the Brill transition temperature in PA66CN3 is at about 150 °C, which is 20 °C lower than that in PA66.

The lower Brill transition temperature of PA66CN3 can be attributed to the strong interaction between polyamide chains and surfaces of silicate layers. As we know, the Brill transition is induced by the thermal expansion of crystalline lattice; the γ phase is favorable in higher temperature. We have demonstrated in earlier paragraph that the addition of silicate layers favors the formation of the γ phase. With increasing annealing temperature, the mobility of molecular chains increases, the transition from the α phase to the γ phase is easier under the existence of silicate layers.

4. Conclusion

A new kind of organophilic clay was obtained through co-intercalation of epoxy resin and alkylammonium into Na-MMT. PA66CN were prepared with this kind of organophilic clay by a twin-screw extruder. In this nanocomposite system, the silicate layers were dispersed homogeneously and nearly exfoliated in PA66 matrix that was the result of the strong interaction between epoxy and PA66. The introduction of silicate layers induced the appearance of the γ phase in PA66CN at room temperature, more clay loadings would amplify this phenomenon; the addition of clay also changed the structure of the α crystalline phase. The presence of silicate layers increased the crystallization rate and had a strong hetero phase nucleation effect on PA66 matrix. The lower Brill transition temperature of PA66CN can be attributed to the strong interaction between polyamide chains and surfaces of silicate layers.

References

[1] Pinnavaia TJ. Science 1983;220:365.
[2] Messersmith PB, Giannelis EP. Chem Mater 1994;6:1719.
[3] Messersmith PB, Giannelis EP. J Polym Sci, Polym Chem 1995;33:1047.
[4] Usuki A, Kojima Y, Kawasumi M, Okada A, Fukushima Y, Kurauchi T, Kamigaito O. J Mater Res 1993;8:1179.
[5] Yano K, Usuki A, Kurauchi T, Kamigaito O. J Polym Sci, Polym Chem 1993;31:2493.
[6] Burnside SD, Giannelis EP. Chem Mater 1994;6:2216.
[7] Vaia RA, Vasudevan S, Krawiec W, Scanlon LG, Giannelis EP. Adv Mater 1995;7:154.
[8] Aranda P, Ruiz-Hitzky E. Chem Mater 1992;4:1395.
[9] Wu J, Lerner MM. Chem Mater 1993;5:835.
[10] Gilman JW. J Appl Clay Sci 1999;15:31.
[11] Vaia RA, Price G, Ruth PN, Nguyen HT. J Appl Clay Sci 1999;15:67.
[12] Kojima Y, Usuki A, Kawasumi M, Okada A, Kurauchi T, Kamigaito O. J Polym Sci, Polym Chem 1993;31:983.
[13] Kojima Y, Usuki A, Kawasumi M, Okada A, Kurauchi T, Kamigaito O, Kaji K. J Polym Sci, Polym Phys 1994;32:625.
[14] Kojima Y, Usuki A, Kawasumi M, Okada A, Kurauchi T, Kamigaito O, Kaji K. J Polym Sci, Polym Phys 1995;33:1039.
[15] Messersmith PB, Giannelis EP. Chem Mater 1993;5:1064.
[16] Chen G, Yao K, Zhao J. J Appl Polym Sci 1999;73:425.
[17] Mehrotra V, Giannelis EP. Solid State Commun 1991;77:155.
[18] Kim JW, Kim SG, Choi HJ, Jhon MS. Macromol Rapid Commun 1999;20:450.
[19] Wu Q, Xue Z, Wang F. Polymer 2000;41:2029.
[20] Mehrotra V, Giannelis EP. Solid State Commun 1992;51:115.
[21] Padmanada T, Kaviratna D, Pinnavaia TJ. Chem Mater 1994;6:573.
[22] Yano K, Usuki A, Kurauchi T. J Polym Sci, Polym Chem 1997;35:2289.
[23] Vaia RA, Ishii H, Giannelis EP. Chem Mater 1995;5:1694.
[24] Moet A, Akelah A. Mater Lett 1993;18:97.
[25] Maxfield M, Christiani BR, Murthy SN, Tuller H. US Patent 5,385,776; 1995.
[26] Liu L, Qi Z, Zhu X. J Appl Polym Sci 1999;71:1133.
[27] Kawasumi M, Hasegawa N, Kato M, Usuki A, Okada A. Macromolecules 1997;30:6333.
[28] Reichert P, Kressler J, Thomann R, Mulhaupt R, Stoppelmann G. Acta Polym 1998;49:116.
[29] Ruiz-Hitzky E, Aranda P. Adv Mater 1990;2:545.
[30] Wong S, Vaia RA, Giannelis EP, Zax DB. Solid State Ionics 1996;86–88:547.
[31] Aranda P, Ruiz-Hitzky E. J Appl Clay Sci 1999;15:119.
[32] Oriakhi CO, Zhang X, Lerner MM. J Appl Clay Sci 1999;15:109.
[33] Akelah A, Kelly P, Qutubuddin S, Moet A. Clay Miner 1994;29:169.
[34] Wang MS, Pinnavaia TJ. Chem Mater 1994;6:468.
[35] Wang Z, Pinnavaia TJ. Chem Mater 1998;10:3769.
[36] Chen TK, Tien YI, Wei KH. J Polym Sci, Part A: Polym Chem 1999;37:2225.
[37] Ho J, Wei K. Macromolecules 2000;33:5181.
[38] Kyotani M, Mitsuhashi S. J Polym Sci, Part A-2 1972;10:1497.
[39] Abu-isa I. J Polym Sci, A-1 1971;9:199.
[40] Hiramatsu N, Hirakawa S. Polym J 1982;14:165.
[41] Dasgupta S, Hammond WB, Goddard WA. J Am Chem Soc 1996;118:12291.
[42] Brill R. J Prakt Chem 1942;161:49.
[43] Hirschinger J, Miura H, Gardner KH, English AD. Macromolecules 1990;23:2153.
[44] Ramesh C, Keller A, Eltink SJEA. Polymer 1994;35:2483.
[45] Murthy NS, Curran SA, Aharoni SM, Minor H. Macromolecules 1991;24:3215.
[46] Vasanthan N, Murthy NS, Bray RG. Macromolecules 1998;31:8433.
[47] Starkweather HW, Jones GA. J Polym Sci, Polym Phys Ed 1981;19:467.
[48] Ramesh C. Mcaromolecules 1999;32:3721.
[49] Kojima Y, Matsuoka T, Takahashi H, Kurauchi T. J Appl Polym Sci 1994;51:683.
[50] Kojima Y, Usuki A, Kawasumi M, Okada A, Fukushima Y, Kurauchi T, Kamigaito O. J Mater Res 1993;8:1185.
[51] Mathias LJ, Davis RD, Jarrett WL. Macromolecules 1999;32:7958.
[52] Akkepeddi MK. ANTEC 99 Conference, New York; May 1999. p. 1619.
[53] Lincoln DM, Vaia RA, Wang ZG, Hsiao BS. Polymer 2001;42:1621.
[54] Jimenez G, Ogata N, Kawai H, Ogihara T. J Appl Polym Sci 1997;64:2211.
[55] Ogata N, Kawakage S, Ogihara T. Polymer 1997;38:5115.